Probing AGN Broad Line Regions with LAT Observations of FSRQs

Jennifer Carson and Jim Chiang, Stanford Linear Accelerator Center

Introduction

The LAT is expected to detect gamma-ray emission from over a thousand active galaxies, many of which will be flat spectrum radio quasars (FSRQs). A commonly assumed ingredient of leptonic models of FRSQs is the contribution to the gamma-ray flux from external inverse-Compton (EIC) scattering of photons from the broad line region (BLR) material by relativistic electrons and positrons in the jet. In this poster we explore two specific ways that LAT spectra of FSRQs can constrain the BLR geometry and optical depth.

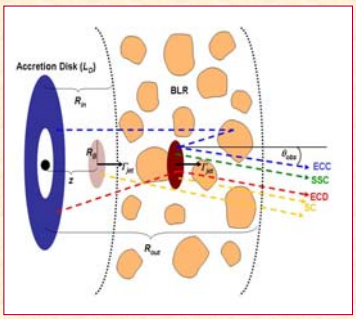

Figure 1.

The model of Böttcher *et al.* (1997) and Böttcher & Bloom (2000) form the basis for these analyses. In this model (see **figures 1 and 3**), pair plasma blobs are instantaneously injected into a cylindrical jet structure with bulk relativistic motion. The electrons have an initial power-law distribution over a range of energies (γ_{min}, γ_{max}). A spherical shell of material of Thomson depth τ represents the BLR. The following radiation processes are included: synchrotron emission (**SC**), inverse-Compton scattering of synchrotron photons (**SSC**), inverse-Compton scattering of radiation from the accretion disk entering the jet directly (**ECD**), and inverse-Compton scattering of accretion disk radiation scattered off broad-line region clouds (**ECC**). The particle distributions are evolved self-consistently as the blob cools.

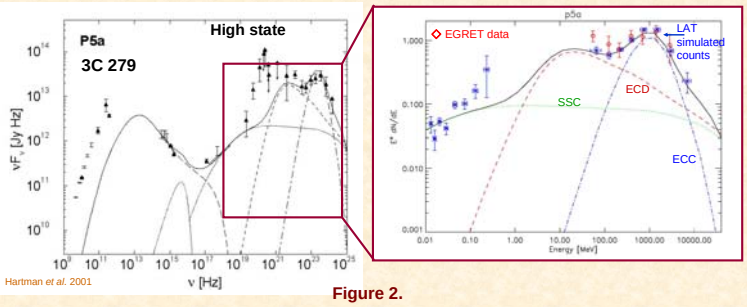

Figure 2.

Figure 2 shows an example of a month of LAT observations of 3C 279 (blue points, right figure), assuming the telescope is operating in its normal survey mode. The input model is taken from Hartman *et al.* (2001, left figure), and the simulation time matches these observations. Galactic and extragalactic diffuse emissions were included in the simulations. **The ECD, ECC, and SSC components all contribute distinct features to the high-energy SED. When the source is in a high state, the LAT counts trace the structure around the emission peak.**

The signature of the BLR geometry in the LAT SED

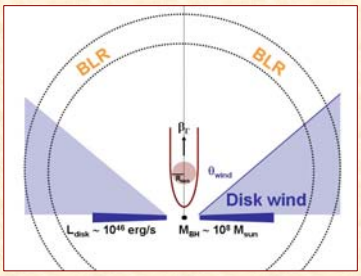

Figure 3.

Past modeling of the ECC emission has considered only a fairly simple geometry for the BLR material: Thomson or resonant line scattering gas that is spherically distributed about the central black hole. However, optical and UV observations of Seyfert galaxies and radio-quiet quasars, as well as theoretical models, suggest that the BLR material may have a very different geometry, such as an equatorial disk wind. To test this hypothesis, we have modified the electron cooling code developed by M. Böttcher to generalize the BLR geometry. We can model the disk wind by introducing an angular dependence (θ_{wind}) into the ECC calculations and evacuating a conical area around the jet (see **figure 3**). The geometry of the remaining region, with θ_{wind} > ~30°, is similar to a wind geometry. We also set the inner radius to $100R_g$ (7×10^{-6} pc for a black hole mass of 1.5×10^8 M_{sun}), adopt $\tau_{wind} = 0.5$, and introduce a density gradient $n \sim r^{-2}$.

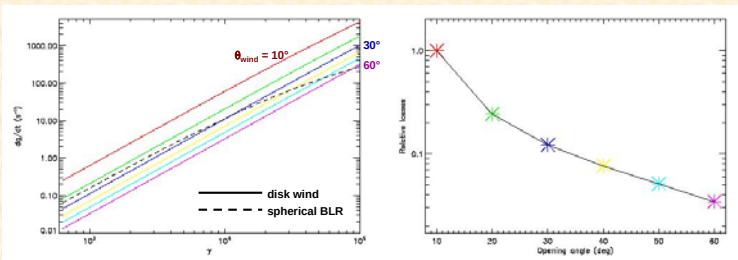

Figure 4. The single-electron energy loss rate due to ECC scattering vs. electron energy γ for opening angles θ_{wind} between 10° and 60° in 10° increments. The dashed line shows the ECC losses for a standard spherical BLR with inner and outer radii of 0.1 and 0.4 pc, respectively, and an optical depth τ = 0.1.

Figure 5. The relative single electron energy loss ratios due to the disk wind as a function of θ_{wind}.

We find:

1. The electron energy losses in the disk wind case are comparable to the electron losses in the spherical BLR case – that is, **the disk wind *can* substantially contribute to the cooling – for θ_{wind} < ~40° (figure 3).** Of course, this limit depends on the other parameters describing the disk and central black hole.
2. **The amount of cooling from a disk wind decreases substantially with opening angle, a factor of ~2 between θ_{wind} = 30° and θ_{wind} = 60° (figure 4).**
3. **The electron losses in the case of a spherical wind have a different energy dependence than the disk wind losses, so the observed spectra can evolve differently in the two cases, assuming these losses dominate the cooling.** We are currently working to quantify the effects of the disk geometry on the observed spectrum.

The signature of BLR cooling in the LAT SED

The observed ECC flux depends more strongly on the Doppler factor D than the observed SSC emission: $F_{\nu,ECC} \sim D^{4+2\alpha}$ and $F_{\nu,SSC} \sim D^{3+\alpha}$, where α = energy spectral index (Dermer 1995). Between observing angles of 2° and 15° the observed ECC flux will decrease by about an order of magnitude relative to the SSC flux. Therefore, even at moderate viewing angles, the SSC emission likely will dominate the observed high-energy emission even when there is a lot of BLR material. Here we investigate the effects of ECC cooling on the SSC spectrum.

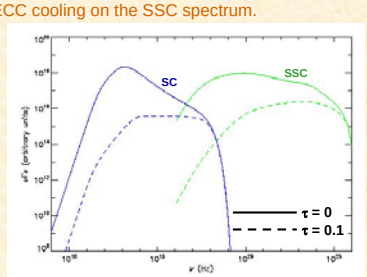

Figure 6. Time-averaged synchrotron (blue) and SSC (green) spectra for τ=0 (solid) and τ=0.1(dashed).

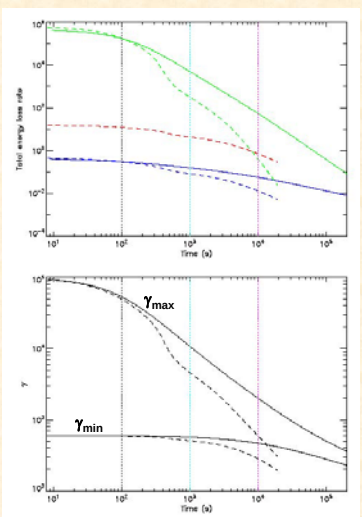

Figure 7. The electron energy loss rate, integrated over all electron energies, vs. time, for synchrotron cooling (blue), SSC cooling (green), and ECC cooling (red), and for τ=0 (solid) and τ=0.1 (dashed).

Figure 8. The evolution of γ_{min} and γ_{max}, the low- and high-energy cutoffs in the electron distribution, vs. time, for τ=0 (solid) and τ=0.1 (dashed).

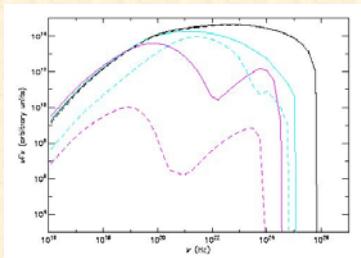

Figure 9. Snapshot SSC spectra at the three times indicated in **figure 7**, for τ=0 (solid) and τ=0.1 (dashed).

We find:

1. **ECC cooling can significantly affect the electron distributions even when it is not the dominant overall source of electron energy losses (e.g., at 10^3 s in figures 7 and 8).**
2. **Consequently, even at larger observing angles, where the ECC contribution is strongly suppressed relative to that of the SSC, the signatures of strong ECC cooling can still be clearly seen in both the lower and higher energy components of the observed SED (figures 6 and 9).**